J. Fluid Mech. (2025), *vol.* 1019, A61, doi:10.1017/jfm.2025.10648

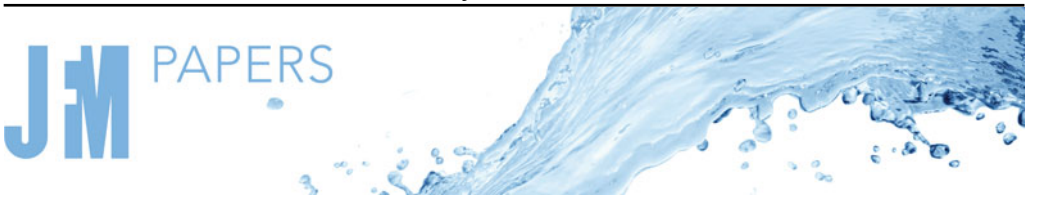

Behaviour of finite-size floating particles in free-surface turbulence

Henri Roland Sanness Salmon[1], **Kelken Chang**[1], **Claudio Mucignat**[2] and **Filippo Coletti**[1]

[1]Department of Mechanical and Process Engineering, ETH Zürich, Zürich, Switzerland

[2]Swiss Federal Laboratories for Materials Science and Technology (Empa), Dübendorf, Switzerland

Corresponding author: Henri Roland Sanness Salmon, rsanness@ethz.ch

(Received 8 July 2025; revised 21 August 2025; accepted 23 August 2025)

Motivated by the need for a better understanding of marine plastic transport, we experimentally investigate finite-size particles floating in free-surface turbulence. Using particle tracking velocimetry, we study the motion of spheres and discs along the quasi-flat free-surface above homogeneous isotropic grid turbulence in open channel flows. The focus is on the effect of the particle diameter, which varies from the Kolmogorov scale to the integral scale of the turbulence. We find that particles of size up to approximately one-tenth of the integral scale display motion statistics indistinguishable from surface flow tracers. For larger sizes, the particle fluctuating energy and acceleration variance decrease, the correlation times of their velocity and acceleration increase, and the particle diffusivity is weakly dependent on their diameter. Unlike in three-dimensional turbulence, the acceleration of finite-size floating particles becomes less intermittent with increasing size, recovering a Gaussian distribution for diameters in the inertial subrange. These results are used to assess the applicability of two distinct frameworks: temporal filtering and spatial filtering. Neglecting preferential sampling and assuming an empirical linear relation between the particle size and its response time, the temporal filtering approach is found to correctly predict the main trends, though with quantitative discrepancies. However, the spatial filtering approach, based on the spatial autocorrelation of the free-surface turbulence, accurately reproduces the decay of the fluctuating energy with increasing diameter. Although the scale separation is limited, power-law scaling relations for the particle acceleration variance based on spatial filtering are compatible with the observations.

Key words: particle/fluid flows, waves/free-surface flows, dispersion

1. Introduction

Since the beginning of the plastic industry in the 1950s, it is estimated that roughly ten billion metric tons (10^{13} kg) of plastics have been produced worldwide, more than half of which have been produced in the last twenty years only (Geyer, Jambeck & Law 2017). Millions of tons of such plastics, the majority of which are positively buoyant, enter the ocean every year in the form of small debris (Geyer *et al.* 2017). While much attention has been devoted to micro-plastics smaller than 5 mm, recent estimates indicate that 95 % of the mass of buoyant marine plastics is accounted for by macro-plastics larger than 25 mm (Kaandorp *et al.* 2023), which are much greater than the dissipative scales of the turbulence in the upper ocean (Jiménez 1997). Therefore, to devise predictive dispersion models and sequestration strategies for this harmful pollution, it is imperative to reach a predictive understanding of the transport of relatively large floating objects. This requires merging two challenging branches in the study of turbulence: its behaviour along a free-surface and its ability to transport finite-size particles. Recent studies have posed fundamental related questions in the context of physical oceanography, considering individual and collective properties of floating particles along with the effects of currents, wind, waves and the Earth's rotation (Beron-Vera 2024; Bonner, Beron-Vera & Olascoaga 2024).

The goal of the present experimental study is to gain insight into the Lagrangian transport of particles of different sizes floating on the quasi-flat free-surface above homogeneous isotropic turbulence, in the absence of surface stresses and significant waves. As the literature on the different involved areas is vast, in the following, we briefly summarise only the background information which is particularly relevant to this work.

1.1. *Turbulent dispersion*

The modelling of Lagrangian turbulent dispersion originates from the theory of Taylor (1922) for the evolution in time t of the position x of a fluid parcel released at time t_0 from a point source in stationary homogeneous isotropic turbulence. The mean square displacement $\langle X^2\rangle(t) = \langle [x(t_0) - x(t)]^2\rangle$ is related to the Lagrangian velocity autocorrelation coefficient $R_u^L(\tau) = \langle u(t_0+\tau)u(t_0)\rangle / \langle u^2\rangle$ via:

$$\langle X^2\rangle(t) = 2\langle u^2\rangle \int_0^t \int_0^{t'} R_u^L(\tau)\,\mathrm{d}\tau\,\mathrm{d}t'. \tag{1.1}$$

Here, $\langle\cdot\rangle$ denotes ensemble averaging, u is the fluctuating velocity, $\tau = t - t_0$ is the time lag and only one component of motion is considered for simplicity of notation. For times much larger than the integral time scale $T_L = \int_0^\infty R_u^L(\tau)\,\mathrm{d}\tau$, $R_u^L(\tau)$ tends to zero and $\langle X^2\rangle(t) = 2\langle u^2\rangle T_L t$. This implies that the long-time turbulent dispersion behaves as a Brownian process with diffusivity:

$$K_t = \frac{1}{2}\frac{\mathrm{d}}{\mathrm{d}t}\langle X^2\rangle(t) = \langle u^2\rangle T_L. \tag{1.2}$$

Taylor's theory finds wide applications in atmospheric sciences and oceanography (Griffa 1996; Wilson & Sawford 1996), and it can be extended to inhomogeneous flows upon appropriate stationarisation of the velocity (Batchelor 1957; Viggiano *et al.* 2021). The crux of the problem is evaluating $R_u^L(\tau)$: this is challenging to measure, as it requires reconstructing trajectories of duration longer than T_L while resolving fine temporal fluctuations associated with the highly intermittent Lagrangian acceleration a (Toschi & Bodenschatz 2009). Indeed, significant efforts have been made to model this quantity. Taylor (1922) assumed a simple exponential, $R_u^L(\tau) = \mathrm{e}^{-\tau/T_L}$, which captures

the long-time decay but not the short-time kinematics $R_u^L(\tau) = 1 - \langle a^2\rangle\tau^2/2\langle u^2\rangle$. This is accounted for by the two-time model proposed by Sawford (1991) and adopted in several later studies (Mordant *et al.* 2004*b*; Jung, Yeo & Lee 2008; Huck, Machicoane & Volk 2019; Berk & Coletti 2021, 2024; Salmon *et al.* 2023):

$$R_u^L(\tau) = \frac{T_1 \mathrm{e}^{-\tau/T_1} - T_2 \mathrm{e}^{-\tau/T_2}}{T_1 - T_2}. \tag{1.3}$$

Here, T_1 and T_2 are associated with the integral and dissipative time scales of the turbulence, respectively. Sawford (1991) modelled the acceleration of fluid particles with a second-order autoregressive equation in which the random perturbation is time-correlated and therefore differentiable. Thus, the kinematic relationship $\langle a^2\rangle R_a^L(\tau) = -\langle u^2\rangle \mathrm{d}^2 R_u^L(\tau)/\mathrm{d}\tau^2$ (Tennekes & Lumley 1972) can be used to evaluate the Lagrangian acceleration autocorrelation coefficient $R_a^L(\tau) = \langle a(t_0+\tau)a(t_0)\rangle/\langle a^2\rangle$ (Sawford 1991; Huck *et al.* 2019):

$$R_a^L(\tau) = \frac{T_1 \mathrm{e}^{-\tau/T_2} - T_2 \mathrm{e}^{-\tau/T_1}}{T_1 - T_2}. \tag{1.4}$$

For fluid tracers, $R_a^L(\tau)$ decays over time scales comparable to the Kolmogorov time τ_η (Yeung & Pope 1989; Voth *et al.* 2002).

1.2. *Inertial particles in turbulence*

Being purely based on kinematics, Taylor's theory applies to fluid tracers as well as inertial particles, i.e. objects too dense and/or too large to follow the fluid flow (Balachandar & Eaton 2010; Brandt & Coletti 2022). The behaviour of small inertial particles (i.e. with diameter d_p smaller than the Kolmogorov scale η) is usually rationalised in terms of the Stokes number $St = \tau_p/\tau_\eta$, where τ_p is the particle response time. As long as the particle Reynolds number $Re_p = \|\boldsymbol{u}_s\| d_p/\nu$ is small, the condition $d_p < \eta$ warrants the approximate validity of Stokes' drag formulation (Clift, Grace & Weber 2005). Here, ν is the kinematic viscosity of the fluid and $\boldsymbol{u}_s = \boldsymbol{u}_{fp} - \boldsymbol{u}_p$ is the slip between the fluid velocity at the particle location $\boldsymbol{u}_{fp}$ and the particle velocity $\boldsymbol{u}_p$. Depending on St, the particle motion has been shown to depart from the fluid flow due to two mechanisms: preferential sampling of regions of high-strain and low-vorticity, prevalent for $St < 1$ (Maxey 1987; Squires & Eaton 1991); and inertial filtering of small-scale/high-frequency turbulent fluctuations, dominant for $St > 1$ (Bec *et al.* 2006).

The inertia of small particles stems from their density ρ_p. When this is much larger than the fluid density ρ, drag and gravity (of acceleration field $\boldsymbol{g}$) dominate over unsteady forces such as added mass, stress gradient and history force (Balachandar 2009; Ling, Parmar & Balachandar 2013). The particle is then often conceptualised as a point mass, and its equation of motion reads:

$$\frac{\mathrm{d}\boldsymbol{u}_p}{\mathrm{d}t} = \frac{\boldsymbol{u}_{fp} - \boldsymbol{u}_p}{\tau_p} + \boldsymbol{g}. \tag{1.5}$$

Neglecting gravity and assuming an exponential decay of $R_u^L(\tau)$, Tchen (1947) showed how (1.5) implies that u_p is obtained from low-pass filtering u_{fp} with a cutoff frequency of τ_p^{-1}. By assuming that u_{fp} is statistically indistinguishable from the unconditional fluid velocity u, they derived

$$\langle u_p^2\rangle = \frac{1}{1 + \tau_p/T_L}\langle u^2\rangle. \tag{1.6}$$

Csanady (1963) and Hinze (1975) used similar but less restrictive assumptions to build a framework later extended by Wang & Stock (1993), Jung *et al.* (2008) and Berk & Coletti (2021), among others. In particular, assuming the form (1.3) for the Lagrangian autocorrelation coefficient of u_{fp}, closed expressions for the particle fluctuating energy $\langle u_p^2 \rangle$, acceleration variance $\langle a_p^2 \rangle$ and velocity correlation time $T_p = \int_0^\infty R_{u_p}^L(\tau)\,\mathrm{d}\tau$ (where $R_{u_p}^L(\tau)$ is the Lagrangian correlation coefficient of u_p) can be derived (see Jung *et al.* 2008; Berk & Coletti 2021):

$$\langle u_p^2 \rangle = \langle u_{fp}^2 \rangle \left[1 - \frac{St^2}{(T_1/\tau_\eta + St)(T_2/\tau_\eta + St)} \right], \tag{1.7}$$

$$\langle a_p^2 \rangle = \frac{\langle u_{fp}^2 \rangle / \tau_\eta^2}{(T_1/\tau_\eta + St)(T_2/\tau_\eta + St)}, \tag{1.8}$$

$$T_p = \frac{(T_1/\tau_\eta + St)(T_2/\tau_\eta + St)(T_1 + T_2)}{(T_1/\tau_\eta + St)(T_2/\tau_\eta + St) - St^2}, \tag{1.9}$$

where now T_1 and T_2 are the time scales in the expression of the Lagrangian autocorrelation coefficient of u_{fp} (see Sawford (1991) and Huck *et al.* (2019)). In the following, we will refer to this framework as temporal filtering. It predicts that the variance of the particle fluctuating energy and acceleration, $\langle u_p^2 \rangle$ and $\langle a_p^2 \rangle$, respectively, decrease with increasing St; while the velocity correlation time T_p grows and the diffusivity $K_p = \langle u_p^2 \rangle T_p$ remains essentially constant. Since extreme turbulent fluctuations are short-lived, this view also predicts that acceleration intermittency, quantified by the flatness $\langle a_p^4 \rangle / \langle a_p^2 \rangle^2$, decreases with St. By modelling u_{fp}, this approach can incorporate the effect of preferential sampling as well as trajectory-crossing, i.e. the particle drift through the turbulence due to body forces such as gravity (Csanady 1963; Wang & Stock 1993); see also Mathai, Lohse & Sun (2020) for the analogous effect on light particles. While simplified, this framework has been shown to capture important trends of the particle behaviour when $d_p < \eta$ and $\rho_p/\rho \gg 1$ (see, e.g. Bec *et al.* (2006), Jung *et al.* (2008), Ireland, Bragg & Collins (2016), Mehrabadi *et al.* (2018) and Berk & Coletti (2021, 2024)).

Developing a similar framework for particles of finite-size and with a density comparable to (or smaller than) that of the fluid would be desirable, but it poses numerous difficulties. First, for $d_p > \eta$, Stokes drag cannot be assumed and a closed form for τ_p is not available. In particular, the power-law dependence $\tau_p \sim d_p^2$ (or $St \sim (d_p/\eta)^2$) leads to large overestimations, especially when the particle Reynolds number is not small. Moreover, for moderate density ratios, unsteady forces may be comparable to drag, complicating the question of how the particle responds to changes in the surrounding fluid flow. The common proxy is the correlation time scale of a_p, $\tau_p \sim \int_0^{T_0} R_{a_p}^L(\tau)\,\mathrm{d}\tau$, where T_0 is the zero-crossing time of the Lagrangian autocorrelation coefficient of the particle acceleration $R_{a_p}^L(\tau)$ (see, e.g. Calzavarini *et al.* (2009) and Volk *et al.* (2011)). Additionally, independent of density, for large (finite-size) particles, u_{fp} and u_s are loosely defined, requiring *ad hoc* heuristics based on the flow surrounding the particle (Kidanemariam *et al.* 2013; Uhlmann & Doychev 2014). Moreover, when $\rho_p/\rho \leqslant 1$, unsteady forces are significant. The point-particle equation of motion for neutrally buoyant particles then predicts that $\langle a_p^2 \rangle$ would increase or remain approximately constant with d_p/η (Calzavarini *et al.* 2009; Homann & Bec 2010). This is at odds with experimental measurements and particle-resolved simulations of neutrally buoyant particles, which show how increasing d_p/η leads to decreasing $\langle a_p^2 \rangle$, as well as increasing T_p and τ_p (Voth

et al. 2002; Qureshi *et al.* 2007, 2008; Volk *et al.* 2008; Brown, Warhaft & Voth 2009; Homann & Bec 2010; Volk *et al.* 2011; Uhlmann & Chouippe 2017; Fan *et al.* 2024).

To address the effect of finite-size, Calzavarini *et al.* (2009) proposed to include Faxén corrections, thus incorporating the non-uniformity of the flow at the particle scale by filtering it over the particle's surface (to estimate drag) and volume (to estimate added mass and stress gradient forces). This produces qualitatively correct trends for neutrally buoyant particles, though it underpredicts the effects of d_p/η (Volk *et al.* 2011; Uhlmann & Chouippe 2017). The interpretation is that the particle motion is driven by turbulent fluctuations occurring at their scale. In other words, finite-size particles are assumed to apply a spatial filtering (or coarse-graining) of the local turbulence (Qureshi *et al.* 2007; Calzavarini *et al.* 2009; Jiang *et al.* 2022; Fan *et al.* 2024). For particle sizes in the inertial subrange, $L \gg d_p \gg \eta$ (L being the integral length scale), velocity fluctuations at the particle scales are thus expected to scale according to the phenomenology put forward by Kolmogorov (1941), $\langle [u(x_0 + d_p) - u(x_0)]^2 \rangle \sim (\varepsilon d_p)^{2/3}$ (where ε is the turbulent dissipation rate), yielding $(\langle u^2 \rangle - \langle u_p^2 \rangle)/\langle u^2 \rangle \sim (d_p/\eta)^{2/3}$, $\langle a_p^2 \rangle / \langle a^2 \rangle \sim (d_p/\eta)^{-2/3}$ and $\tau_p/\tau_\eta \sim (d_p/\eta)^{2/3}$. While those are compatible with the observations, the limited available data cannot exclude other scaling behaviours (Voth *et al.* 2002; Qureshi *et al.* 2007; Homann & Bec 2010; Volk *et al.* 2011; Uhlmann & Chouippe 2017; Fan *et al.* 2024). Moreover, in keeping with the distribution of velocity increments at increasing separations, the spatial filtering framework implies that the particle acceleration (regardless of particle density) becomes less intermittent for larger d_p (Xu *et al.* 2007; Brown *et al.* 2009). This is in contrast with experiments and particle-resolved simulations of neutrally buoyant particles, which report high flatness of a_p even for $d_p/\eta \gg 1$ (Qureshi *et al.* 2007, 2008; Xu & Bodenschatz 2008; Brown *et al.* 2009; Homann & Bec 2010; Bellani & Variano 2012). Even when a reduction of intermittency with particle size was reported, the acceleration flatness was still found to be far higher than the Gaussian limit (Volk *et al.* 2011).

The above-mentioned works on finite-size neutrally buoyant particles were concerned with three-dimensional (3-D) turbulence. Ouellette, O'malley & Gollub (2008) investigated the motion of spheres in a two-dimensional (2-D) chaotic flow, and found the larger ones had a somewhat larger diffusivity. However, Xia *et al.* (2019) found that the diffusivity of discs floating on wave-driven 2-D turbulence decreased when their diameter increased. Therefore, the behaviour of (quasi-) neutrally buoyant finite-size particles in free-surface turbulence (which, as we describe later, shares similarities with both 2-D and 3-D turbulence) remains an open question.

1.3. *Free-surface turbulence*

Most previous studies concerned with free-surface turbulence have focused on the effect of the boundary conditions on the sub-surface flow; see seminal studies by Hunt & Graham (1978), Perot & Moin (1995), Shen *et al.* (1999) and Magnaudet (2003), among several others recently reviewed by Ruth & Coletti (2024). In particular, the kinematic boundary condition $u_z = 0$ at $z = 0$ influences a so-called 'blockage layer' of thickness comparable to the integral scale L, increasing the surface-parallel velocity fluctuations at the expense of the vertical fluctuations. Here and in the following, x and y indicate the surface-parallel directions (x being streamwise in the presence of a mean flow) and z, positive upward, is the surface-normal (vertical) direction; u_x, u_y and u_z are the corresponding velocity components. In the limit of large turbulent Reynolds number Re, the behaviour of the Reynolds stresses in the blockage layer is well predicted by the theory of Hunt & Graham (1978) based on rapid-distortion theory (Magnaudet 2003; Ruth & Coletti 2024).

The dynamic boundary condition $\partial u_x/\partial z = \partial u_y/\partial z = 0$, however, imposes that vortex lines reorient to be surface-normal within a surface layer of thickness $LRe^{-1/2}$. This has significant consequences for the dynamics immediately below the free-surface (Shen *et al.* 1999; Guo & Shen 2010; Aarnes *et al.* 2025) but also for the motion along it. Li *et al.* (2025) studied the behaviour of millimetric tracers floating along the quasi-flat free-surface above turbulent water past a square-mesh grid. While the statistics of velocity fluctuations, accelerations and dissipation were similar to those in the bulk, and followed the classic phenomenology of Kolmogorov (1941), the surface-normal vorticity signalled the presence of long-lived vortices (Kumar, Gupta & Banerjee 1998; Lovecchio, Zonta & Soldati 2015). This was later confirmed in the detailed measurements of Qi *et al.* (2025*a*,*b*), who tracked microscopic surface tracers in a homogeneous zero-mean-flow turbulent water tank, highlighting the effect of the dynamic boundary condition on strain-rate and vorticity.

In the absence of significant surfactant effects, the surface velocity field displays a compressibility $\langle(\partial u_z/\partial z)^2\rangle$ comparable to the mean square velocity gradients in the bulk, which in turn influences the dispersion of small floating particles (Boffetta *et al.* 2004; Cressman *et al.* 2004; Lovecchio, Marchioli & Soldati 2013; Li *et al.* 2024, 2025).

1.4. *Focus of the present study*

Despite its relevance, the behaviour of finite-size particles floating in free-surface turbulence has rarely been addressed in fundamental fluid mechanics investigations. Valero *et al.* (2022) studied the behaviour of realistic buoyant litter such as plastic cups, flexible films and face masks in a laboratory flume, highlighting the importance of surface tension and the effect of their size on the transport. In a recent field study, we have reported on the transport of centimetre-sized discs and rods floating in an outdoor meandering stream (Sanness Salmon *et al.* 2023). Compared with millimetre-sized floating tracers, the larger particles were observed to have reduced accelerations and more time-correlated motions, which impacted their diffusivity.

In the present study, we use the experimental facilities employed by Li *et al.* (2025) to study the transport of tracers on the quasi-flat free-surface above homogeneous isotropic grid turbulence, and focus on the behaviour of marginally buoyant particles in a wide range of sizes, $d_p/\eta \in [5, 110]$. We characterise in detail their single-point and two-point/two-time statistics, and discuss to which degree their behaviour is consistent with specific assumptions. We aim to answer the following questions. How does the size of the floating particles affect their motion, in particular, the velocity fluctuations, accelerations and diffusivity? To which extent can the floating particles be modelled as point-particles of a given response time? And to which extent can they be modelled as spatial filters of the underlying turbulent flow?

The rest of the paper is organised as follows: the experimental approach and the parameter space are described in § 2; § 3 presents the results in terms of flow properties below and along the free-surface (§ 3.1) and the particle behaviour (§ 3.2). We then explore to which degree the latter is consistent with the frameworks of temporal filtering (§ 3.3) and spatial filtering (§ 3.4). Section 4 discusses the results, draws conclusions and gives an outlook.

2. Methods

2.1. *Experimental apparatus*

To cover a wide range of parameters, experiments are performed in two recirculating open-channel flumes, one located at ETH Zürich and the other at the Swiss Federal

Facility	H (m)	W (m)	U_s (m s^{-1})	M (mm)	Re_M (-)	Fr (-)	We (-)	Re_λ (-)
ETH	0.400	0.450	0.207	35.0	7 230	0.10	0.06	29
Empa	0.550	1.010	0.270	70.0	18,860	0.12	0.08	43, 84

Table 1. Hydrodynamic parameters characterising the free-surface flow in the two used facilities: water depth H, channel width W, mean surface velocity U_s, square mesh size M, grid Reynolds number Re_M, Froude number Fr, Weber number We and Taylor-scale Reynolds number of the turbulence Re_λ.

Laboratories for Materials Science and Technology (Empa). The two facilities are different in scale but identical in architecture, and the same measurement approaches are used in both, as described in detail by Li *et al.* (2025). A centrifugal pump drives water through an upstream plenum featuring flow conditioning components (perforated stainless-steel plates, polycarbonate honeycombs and stainless-steel screens) before entering a contraction with a 6–1 area ratio. Turbulence is generated by a stainless-steel grid spanning the entire water cross-section of depth H and width W. The grid features squared bars of width d and mesh size M, resulting in a grid solidity $\sigma = (d/M)(2 - (d/M)) = 0.31$. The main hydrodynamic parameters of the two facilities are summarised in table 1. The Reynolds number $Re_M = U_s M/\nu$ and the Froude number $Fr = U_s/\sqrt{gH}$ are based on the mean surface velocity U_s. At the start of each experiment, surface residue is removed with a fine net and a standard surface tension $\gamma = 72$ mN m^{-1} is measured via a Du Noüy ring. The values of Fr and of the Weber number $We = \rho\langle u^2\rangle L/\gamma$ are consistent with the minimal deformation of the water surface, on which only sub-millimetre wave amplitudes are observed. In the Empa facility, two configurations of the flow conditioning components are used, resulting in two different levels of turbulence intensity. Therefore, three cases with different Taylor-scale Reynolds number Re_λ (whose evaluation is detailed in § 3.1) are considered.

Two types of floating particles are considered (table 2): white polypropylene spheres (RGPBalls Srl, $\rho_p = 0.87$ g cm^{-3}) and polypropylene discs ($\rho_p = 0.92$ g cm^{-3}), photographed in figure 1. Their diameters vary in the range $d_p \in [1.6, 30]$ mm, with the smallest spheres used as tracers to characterise the free-surface turbulent flow (see Li *et al.* 2025 for the verification that those particles faithfully follow the flow). In terms of Kolmogorov scales, these tracers correspond to $\sim 8\eta$ and $\sim 5\eta$, for the ETH and Empa facilities, respectively. We remind that for 3-D turbulence, neutrally buoyant spherical particles up to $d_p \sim 5\eta$ behave as flow tracers (Homann & Bec 2010; Fiabane *et al.* 2012; Uhlmann & Chouippe 2017; Berk & Coletti 2024). For free-surface flows, it has been shown that particles up to $d_p \sim 10\eta$ capture most of the turbulent kinetic energy (Nikora *et al.* 2007; Sanness Salmon *et al.* 2023). The discs are produced in-house by laser-cutting 1 mm thick sheets (Vibraplast AG) using a VLS3.50 Desktop Laser (Universal Laser Systems Inc.). The large diameter-to-thickness ratio guarantees that the floating discs remain parallel to the water surface. The particles are mostly submerged, consistent with the weight/buoyancy force balance, which (neglecting surface tension effects) prescribes their fractional submerged volume to be approximately equal to their relative density ρ_p/ρ.

2.2. *Measurement approach*

The sub-surface turbulence properties in the bulk and across the blockage layer are measured by particle image velocimetry (PIV) of 10 μm hollow glass spheres (LaVision GmbH, $\rho_p = 1.10$ g cm^{-3}). This is performed along the mid-span vertical plane and

Particle type	ρ_p/ρ (-)	d_p (mm)	d_p/η (-)	d_p/L (-)
Sphere	0.87	1.6	5.7	0.03
		2.0	6.1, 8.4	0.06, 0.13
		5.0	15.2, 21.1	0.14, 0.32
		7.0	21.2, 29.5	0.20, 0.45
		10.0	30.4, 42.2	0.28, 0.65
Disc	0.92	5.0	15.2	0.14
		7.0	21.2	0.20
		10.0	30.4	0.28
		15.0	45.5	0.43
		20.0	71.7	0.33
		25.0	89.6	0.42
		30.0	107.6	0.50

Table 2. Physical properties and experimental summary of the floating particles including shape, relative density ρ_p/ρ and diameter d_p in dimensional and dimensionless units.

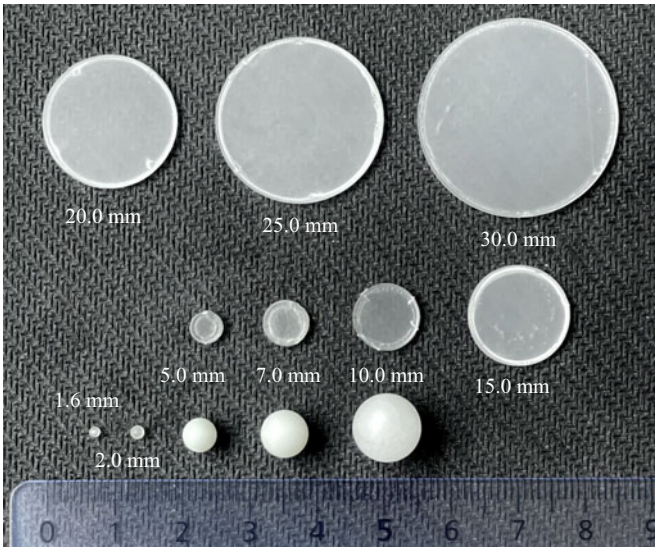

Figure 1. A close-up photograph of the finite-size floating particles; spheres (bottom row) and discs (top and middle row).

several surface-parallel planes as close as ∼1 mm from the free-surface, as described in detail by Li *et al.* (2025).

The properties of the free-surface turbulence and the behaviour of the finite-size particles are obtained by particle tracking velocimetry (PTV) of the floating particles. These are released at the inlet of the test section with a handheld spreader (Gardena GmbH) and collected by a nylon net fixed at the outlet of the test section. Number concentrations that may cause inter-particle interactions are avoided. The particles are imaged by a 12MP CMOS camera (Baumer Ltd, VQXT-120C.HS) mounting Zeiss Milvius lenses. This is suspended above the channel at a downstream location of $x = 30M$ from the grid, pointing downward at the free-surface flow. The position is chosen such that the field of view (FOV) is within a region where equilibrium conditions have been reached and classic scaling relations for homogeneous isotropic turbulence apply (Mohamed & Larue

Facility	fps (Hz)	Resolution (px^2)	Focal length (mm)	Spatial resolution (px mm^{-1})	FOV (m^2)	Imaging range (x/M)
ETH	100	4096 × 2400	35	8.26	0.497 × 0.291	24 to 36
Empa	90	4096 × 3068	21	7.04	0.583 × 0.437	27 to 32

Table 3. Main imaging parameters for the two experimental facilities: frame rate, camera resolution, focal length of the lens, spatial resolution, size of the FOV and non-dimensional distance from the grid spanned by the FOV.

1990; Lavoie, Djenidi & Antonia 2007; Hearst & Lavoie 2014). Two continuous LEDs (GS Vitec GmbH, MultiLED) illuminate the FOV from both ends of the channel. Diffusers are employed to evenly distribute the light along the water surface, and black background panels are positioned on the transparent walls of the test section to improve image contrast. The imaging parameters for the two facilities are summarised in table 3. The camera calibration is realised by imaging a checkerboard pattern kept at the water surface level, which allows correcting for slight barrel distortion (Zhang 2000). The boundaries of the FOV, which is centred at mid-span and covers approximately half of the channel width, are sufficiently far from the channel sidewalls to ensure that the imaged flow is not influenced by the lateral boundary layers.

Particles are identified via image segmentation above an intensity threshold, whose exact value is not consequential thanks to the high contrast. The centroids of contiguous groups of pixels exceeding the threshold are identified via a circle-finder algorithm based on the circular Hough transform (alternative algorithms returning the same results within sub-pixel accuracy). Rare occurrences of adjacent particles are discarded in post-processing, imposing a minimum inter-particle gap of twice the capillary length $\sqrt{\gamma/\rho g} = 2.7$ mm or d_p (whichever is larger). This guarantees that the tracked particles are not significantly influenced by their neighbours.

Particle trajectories are reconstructed using an in-house code implementing a nearest-neighbour PTV algorithm (Baker & Coletti 2019, 2021, 2022; Sanness Salmon *et al.* 2023). For the tracer particles, an advective predictor is used which searches in the radius around the centroid shifted downstream by $\Delta x = \langle U \rangle \Delta t$ (Δt being the inter-frame temporal separation). For particles 5 mm and larger, the advective predictor is unnecessary as the inter-frame displacements are smaller than the particle radius. The particle positions $\boldsymbol{x}_p$, velocities $\boldsymbol{u}_p$ and accelerations $\boldsymbol{a}_p$ are obtained by convolving the trajectories with a Gaussian kernel and its derivatives, removing most of the high-frequency noise (Voth *et al.* 2002; Mordant *et al.* 2004*a*). Here and in the following, the bold typeface indicates vectors associated with the two-dimensional motion along the free-surface. Because tracking floating particles along the quasi-flat free-surface is a robust process, most of the reconstructed trajectories have comparable lengths. Still, to avoid possible biases due to varying trajectory length (Mordant *et al.* 2004*a*; Guala *et al.* 2007), we calculate Lagrangian statistics from trajectories of equal length (180 and 140 frames in the ETH and Empa facilities, respectively), trimming longer trajectories.

As tracking errors are negligible, the uncertainties are mostly associated with the finite number of samples. To yield a number of trajectories sufficient for statistical convergence, between twenty and one hundred measurement runs are conducted for each particle-flow condition combination, with 2700–2900 images acquired in each run. For $d_p \leqslant 7$mm, more than 10 000 trajectories are obtained for each case. The larger particles have a lower yield due to the constraint of avoiding inter-particle interaction, but the statistics are still based on at least 3700 trajectories. Although statistical convergence of the observables

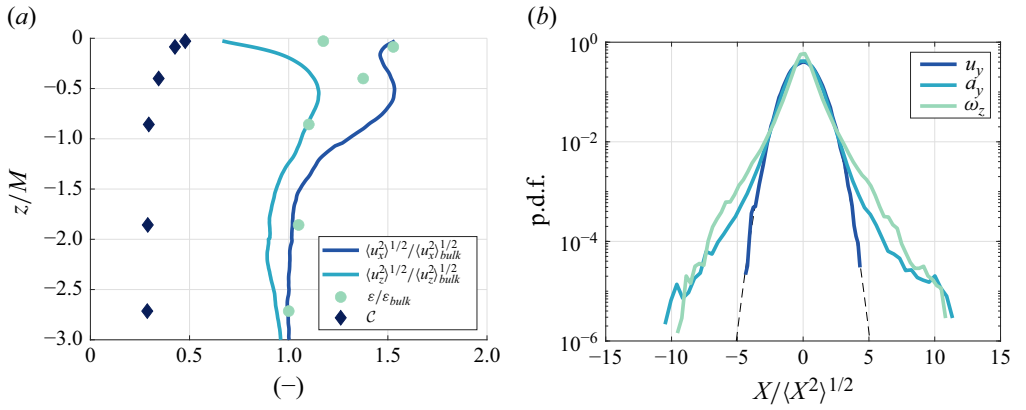

Figure 2. (*a*) Vertical profiles of the sub-surface properties measured by PIV at $Re_\lambda = 29$. (*b*) Corresponding probability distribution functions (p.d.f.s) of the free-surface turbulence properties measured by PTV. The dashed line indicates a normal distribution.

within a few percent is achieved in each experimental run, larger variability is observed between different runs. Therefore, when relevant for the interpretation of the results, the statistical uncertainty is represented with error bars given by the run-to-run standard deviation.

3. Results

3.1. *Properties of the turbulence below and along the free-surface*

For both facilities, the full characterisation of the sub-surface and free-surface flow is reported by Li *et al.* (2025). Here, we provide an account of the main properties, with plots of selected cases to illustrate the flow behaviour.

With the uppermost grid bar located at approximately $z = -0.86M$, turbulence is forced over the entire flow volume. Indeed, the behaviour of the sub-surface turbulence measured by PIV is consistent with the predictions of Hunt & Graham (1978) for the evolution of homogeneous turbulence below a flat free-surface: the root mean square (r.m.s.) of the vertical velocity fluctuations $\langle u_z^2\rangle^{1/2}$ drops to vanishingly small levels approaching the free-surface, while the horizontal one $\langle u_x^2\rangle^{1/2}$ increases. The dissipation rate ε grows in the blockage layer and decreases in the surface layer to approximately recover its bulk value. The compressibility coefficient $\mathcal{C} = \langle(\partial u_i/\partial x_i)^2\rangle/\langle(\partial u_i/\partial x_j)^2\rangle$ (with indices restricted to the surface-parallel components) grows to approach the free-surface condition $\mathcal{C} = 0.5$, implying that the in-plane velocity gradients are uncorrelated (Cressman *et al.* 2004; Boffetta *et al.* 2004). These trends are displayed in figure 2(*a*) for the representative case $Re_\lambda = 29$.

The lateral velocity fluctuations u_y and accelerations a_y of the tracer particles measured by PTV yield the probability distribution functions (p.d.f.s) plotted in figure 2(*b*), normalised by their respective r.m.s. values. The p.d.f. of surface-normal vorticity ω_z is also shown, obtained from Lagrangian tracking of 2 mm long floating rods (see Li *et al.* 2025). The rods' r.m.s. rotation rate was found to be an appropriate proxy for the near-surface ω_z measured via PIV. While u_i are normally distributed, a_i and ω_z display levels of intermittency of the small-scale flow features comparable to those in 3-D turbulence (Qi *et al.* 2025*a*).

Re_λ	u_{rms} (m s^{-1})	ε (m^{2}s^{-3})	L (mm)	T_L (s)	λ (mm)	η (mm)	τ_η (s)
29	0.012	3.2×10^{-4}	15.5	1.23	2.5	0.2	0.06
43	0.010	0.9×10^{-4}	35.1	1.87	4.3	0.3	0.11
84	0.017	1.7×10^{-4}	59.7	2.19	5.0	0.3	0.08

Table 4. Quantities characterising the free-surface turbulence for the three considered Re_λ: r.m.s. velocity fluctuation u_{rms}, mean dissipation rate of turbulent kinetic energy ε, integral length scale L, integral time scale T_L, Taylor micro-scale λ, Kolmogorov length scale η and Kolmogorov time scale τ_η.

The free-surface velocity data are used to obtain Eulerian fields of the mean and r.m.s. fluctuations of the free-surface velocity. The measurements are spatially binned into 5 mm × 5 mm windows, the size of which is chosen to give at least 100 instantaneous vectors for ensemble-averaging. The fluctuations are obtained by subtracting the local mean velocity, which varies by only a few percent within the FOV. Both r.m.s. components are similar, with the anisotropy ratio $\langle u_x^2\rangle/\langle u_y^2\rangle$ in the range of 0.96–1.18. The streamwise decay of the turbulent kinetic energy of the free-surface flow is well described by a power-law decay:

$$\frac{\langle q^2\rangle}{U_s^2} = A\left(\frac{x}{M} - \frac{x_0}{M}\right)^{-m}, \tag{3.1}$$

where $\langle q^2\rangle = \langle \boldsymbol{u}\cdot\boldsymbol{u}\rangle = \langle u_x^2\rangle + \langle u_y^2\rangle$, x_0 is the virtual origin of the grid and the parameter A is determined via a least-square fit. The decay exponent m is found to be close to unity, consistent with results in 3-D turbulence (Mohamed & Larue 1990; Lavoie *et al.* 2007; Hearst & Lavoie 2014; Sinhuber, Bodenschatz & Bewley 2015). The mean dissipation rate along the free-surface is evaluated from the spatial decay of $\langle q^2\rangle$, from which we evaluate free-surface values of the Kolmogorov scales, Taylor microscale $\lambda = \sqrt{15}u_{rms}\tau_\eta$ and $Re_\lambda = u_{rms}\lambda/\nu$, where $u_{rms} = \sqrt{\langle q^2\rangle/2}$. To determine the integral length scales L of the free-surface turbulence, we evaluate the Eulerian velocity correlation coefficient:

$$R_u^E(r) = \frac{\langle \boldsymbol{u}(\boldsymbol{r}_0 + \boldsymbol{r})\cdot\boldsymbol{u}(\boldsymbol{r}_0)\rangle}{\langle q^2\rangle}, \tag{3.2}$$

where the ensemble-averaging is carried out over tracers separated by a distance r from the reference location $\boldsymbol{r}_0$, discretising the separation in bins containing $\mathcal{O}(10^4)$ data points each. An exponential fit to the form $R_u^E(r) = \mathrm{e}^{-r/L}$ yields values of the integral scale consistent with the classic relation $L \sim u_{rms}^3/\varepsilon$ (Tennekes & Lumley 1972). Similarly, the integral time scale T_L is evaluated by fitting an exponential decay to the Lagrangian velocity autocorrelation coefficient, $R_u^L(\tau) = \mathrm{e}^{-\tau/T_L}$. The free-surface turbulence properties for the three considered flow conditions are summarised in table 4.

3.2. *Behaviour of finite-size floating particles*

To describe the kinematics of the finite-size particle motion, only selected components of the free-surface velocity and acceleration are illustrated; the behaviour of both components is quantitatively similar, as expected from the quasi-isotropic nature of the free-surface turbulence.

The p.d.f.s of the lateral velocity fluctuations are plotted in figure 3(*a*), normalised by the respective r.m.s. values, showing a Gaussian distribution for all sizes. Figure 3(*b*) shows how the particle fluctuating energy $\langle u_p^2\rangle = \langle \boldsymbol{u}_p\cdot\boldsymbol{u}_p\rangle$ remains equal to the one of tracers up to approximately $d_p/L = 0.1$ and drops significantly for larger sizes: increasingly large floating particles are less responsive to the underlying fluid fluctuations. In terms of the

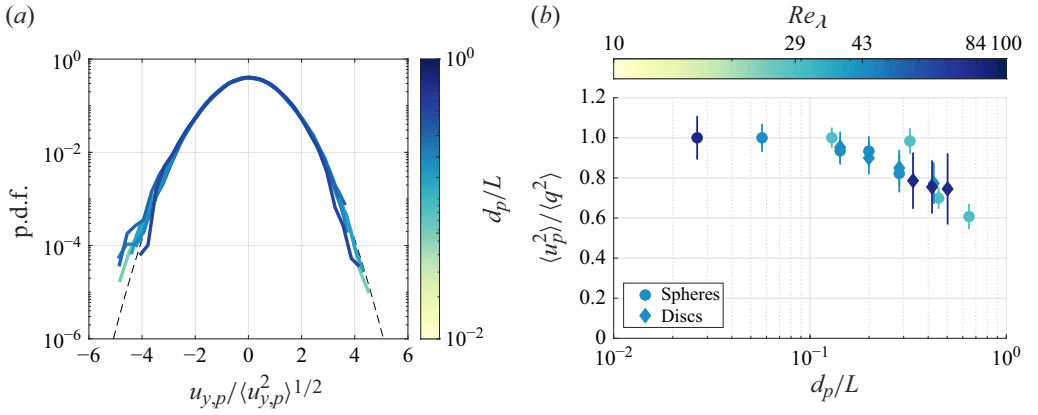

Figure 3. (*a*) P.d.f.s of the lateral velocity fluctuations of the floating particles for $Re_\lambda = 43$. The dashed line indicates a normal distribution. (*b*) Particle fluctuating energy versus dimensionless particle size. Error bars represent the run-to-run standard deviation.

Kolmogorov scale, this corresponds to $d_p/\eta \in [8, 20]$ for the different cases. In general, the reduction of fluctuating energy with increasing particle size agrees with findings in 3-D turbulence (Homann & Bec 2010; Calzavarini *et al.* 2012; Chouippe & Uhlmann 2015; Uhlmann & Chouippe 2017). Our results are comparable, for example, with the experiments of Machicoane *et al.* (2014) who measured an energy reduction of roughly 40 % for very large ($d_p/L \sim 0.5$) neutrally buoyant spherical particles in a von Kármán flow. The fundamental differences between 3-D and free-surface turbulence, however, limit the value of quantitative comparisons. Here and in the following figures, no systematic differences are seen in the behaviour of floating spheres and discs of similar diameter ($Re_\lambda = 43$). This suggests that, for the present level of submergence, the motion of floating particles depends on the near-surface flow and how this is modulated by their spatial extension in the surface-parallel direction. This is consistent with the submerged depth of the particles (estimated from a simple force balance and visually verified), which is at most comparable with the surface layer (Hunt & Graham 1978). Larger particles whose centre of mass resides in the blockage layer may display different dynamics.

The p.d.f.s of the streamwise particle acceleration are reported in figure 4(*a*). Unlike for the velocity fluctuations, the particle size has a clear influence on the shape of the distributions: the intermittency decreases significantly with increasing size, and the acceleration of the larger particles essentially follows a Gaussian distribution. The total acceleration variance $\langle a_p^2\rangle = \langle \boldsymbol{a}_p \cdot \boldsymbol{a}_p\rangle$ remains approximately constant for $d_p/L < 0.1$ and drops for larger sizes (figure 4*b*), and it does so more steeply than the fluctuating kinetic energy. This is likely related to the fact that the fluid accelerations are mostly associated with the fine scales of the turbulence (Toschi & Bodenschatz 2009), as discussed in the following sections.

The degree to which the motion of the finite-size particles is time-correlated is described by the particle velocity autocorrelation coefficient, illustrated in figure 5(*a*) for $Re_\lambda = 29$. The decay rate of $R_{u_p}^L(\tau)$ decreases with particle size, which is quantified by the increase of the correlation time scale T_p. This is estimated by fitting an exponential of the form e^{-t/T_p} to the measurement of $R_{u_p}^L(\tau)$, reported in figure 5(*b*) normalised by the fluid integral time scale T_L. We note that this procedure is associated with significant uncertainty: the accurate measurement of the integral time scales requires integrating over a duration

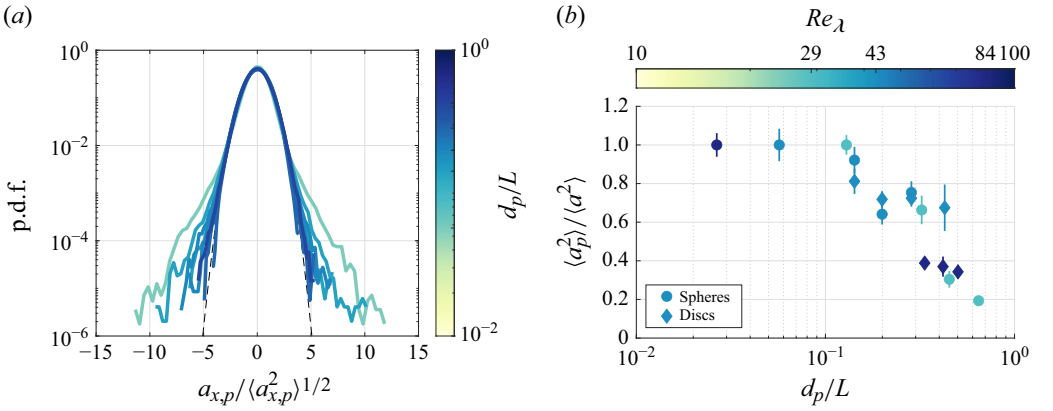

Figure 4. (*a*) P.d.f.s of streamwise acceleration of the floating particles for $Re_\lambda = 43$. The dashed line indicates a normal distribution. (*b*) Particle acceleration variance versus dimensionless particle size. Error bars represent the run-to-run standard deviation.

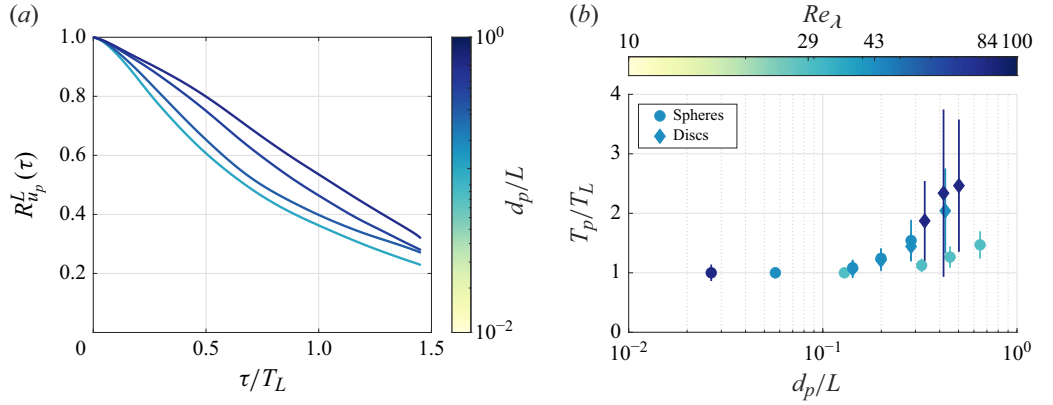

Figure 5. (*a*) Measured Lagrangian particle velocity autocorrelation coefficients for $Re_\lambda = 29$. (*b*) Particle velocity correlation time scale versus dimensionless particle size. Error bars represent the run-to-run standard deviation.

significantly longer than the time scales themselves. This is, however, seldom possible in laboratory experiments due to the limited length of the trajectories (even in the present case, in which most of the trajectories stretch over the entire FOV). Therefore, we rely on the assumption that the autocorrelations decay exponentially (as in Baker & Coletti 2021 and Sanness Salmon *et al.* 2023). The uncertainty associated with possible departures of $R_{u_p}^L(\tau)$ from the measured exponential decay at long times also affects the diffusivity (discussed later), but is not expected to overshadow the reported trends. Similar to the velocity and acceleration, the correlation time scale of particles smaller than $d_p/L = 0.1$ is indistinguishable from the one of the fluid. For larger diameters, an increasing trend of T_p/T_L is apparent: the motion of larger particles is characterised by more time-correlated velocity fluctuations.

3.3. *Comparison with the temporal filtering framework*

In this section, we evaluate the applicability of the temporal filtering framework to the dynamics of the finite-size floating particles. The first step is to evaluate an effective

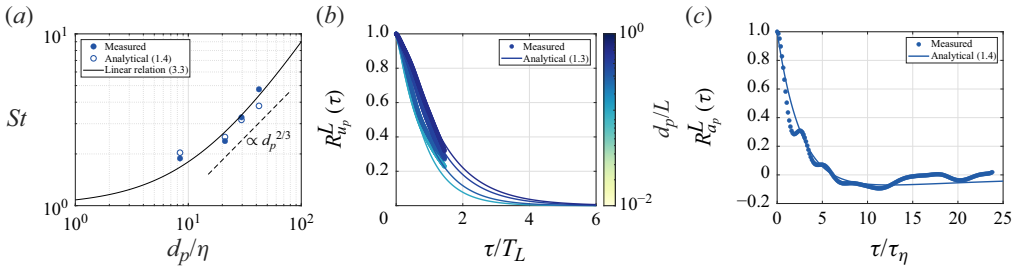

Figure 6. (*a*) Particle Stokes number evaluated by integrating their measured acceleration autocorrelation coefficient (filled symbols) and their equivalent analytical form (1.4) inspired by Sawford (1991) (open symbols). The continuous line is the linear relation (3.3) from Uhlmann & Chouippe (2017) and the dashed line is the 2/3 power-law scaling based on Kolmogorov (1941). (*b*) Lagrangian particle velocity autocorrelation coefficients for $Re_\lambda = 29$ measured by PTV (filled symbols) and their respective analytical form (1.3) (lines). (*c*) Lagrangian particle acceleration autocorrelation coefficient for $d_p/\eta = 21.1$ and $Re_\lambda = 29$ measured by PTV (symbols) and its analytical form (line). The oscillations are due to the small surface waves.

response time τ_p, which can be estimated as the definite integral of $R^L_{a_p}(\tau)$ up to the zero-crossing time T_0 (Calzavarini *et al.* 2009). Measuring the latter, however, is challenging as it requires high temporal resolution and low noise (Machicoane & Volk 2016; Machicoane, Huck & Volk 2017). Inspection of our data indicates that the cases at $Re_\lambda = 29$ provides robust estimates of τ_p, which are plotted in figure 6(*a*) in terms of St (filled symbols).

An alternative, though related strategy is to use an analytical model for $R^L_{u_p}(\tau)$ and differentiate it to obtain $R^L_{a_p}(\tau)$. Following this avenue, we employ the model of Sawford (1991), with two temporal scales that capture the large-scale and dissipative particle dynamics. In the original model, $T_1 = 2\langle u^2\rangle / C_0\varepsilon = \mathcal{O}(T_L)$ and $T_2 = \tau_\eta C_0/2a_0 = \mathcal{O}(\tau_\eta)$, where $a_0 = \langle a^2\rangle \varepsilon^{-3/2}\nu^{1/2}$ and C_0 is the constant in the inertial scaling of the second-order Lagrangian structure function, $S^L_2(\tau) = \langle [u(t_0+\tau) - u(\tau)]^2\rangle = C_0\varepsilon\tau$ (Kolmogorov 1941). By analogy, we define $T_{1,p} = 2\langle u_p^2\rangle / C_{0,p}\varepsilon = \mathcal{O}(T_p)$ and $T_{2,p} = \tau_\eta C_{0,p}/2a_{0,p} = \mathcal{O}(\tau_p)$, where $a_{0,p} = \langle a_p^2\rangle \varepsilon^{-3/2}\nu^{1/2}$ and $C_{0,p}$ is found by fitting the measured structure function of the Lagrangian particle velocity as $S^L_{2,p}(\tau) = C_{0,p}\varepsilon\tau$. The resulting forms of $R^L_{u_p}(\tau)$ and $R^L_{a_p}(\tau)$ (equivalent to (1.3) and (1.4), with $T_{1,p}$ and $T_{2,p}$ in place of T_1 and T_2, respectively) capture reasonably well the behaviour of the measurements, as shown for selected cases in figures 6(*b*) and 6(*c*). Because the model parameters are set based on the measurements, the agreement mostly indicates that the forms (1.3) and (1.4) are appropriate to describe the autocorrelation coefficients. Indeed, the values of St based on integrating the analytical form of $R^L_{a_p}(\tau)$, plotted as open symbols in figure 6(*a*), are in good agreement with those based on the measurements.

Both these strategies require empirical knowledge of the Lagrangian particle velocities and accelerations, while one would like to estimate τ_p based on the turbulence and particle characteristics only. However, as discussed in § 1.2, there is no consensus on the correct expression or even the scaling dependence of τ_p with the particle properties. Here, we test the empirical linear relation

$$St = 1 + 0.08\left(\frac{d_p}{\eta}\right), \tag{3.3}$$

which was shown by Uhlmann & Chouippe (2017) to represent well their particle-resolved simulations and the experiments by Volk *et al.* (2011) in 3-D turbulence. Figure 6(*a*) shows

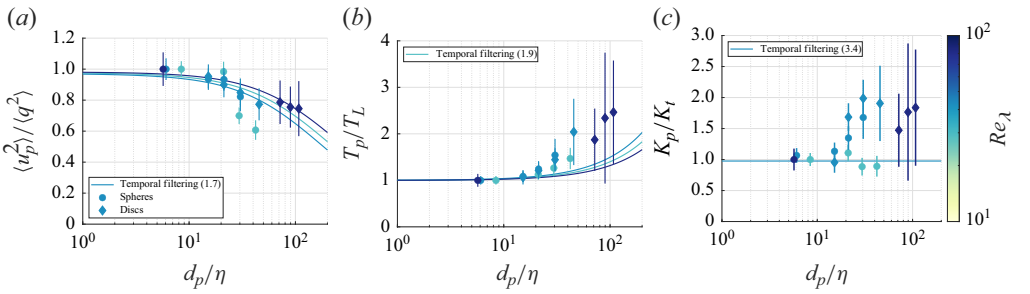

Figure 7. Comparison between measurements (filled symbols) and the temporal filtering framework (lines) for all Re_λ cases; (*a*) particle fluctuating energy (1.7), (*b*) velocity correlation time scale (1.9) and (*c*) particle diffusivity (3.4) versus dimensionless particle size. Error bars represent the run-to-run standard deviation.

that such a relation is also consistent with the behaviour of our finite-size particles floating in free-surface turbulence. Therefore, for simplicity, we will adopt (3.3) in the following analysis. Two remarks are, however, in order. First, (3.3) is expected to overestimate St in the range $d_p/\eta \lesssim 5$, as neutrally buoyant particles of this size are indistinguishable from tracers both in 3-D and free-surface turbulence (Qureshi *et al.* 2007; Volk *et al.* 2011; Berk & Coletti 2024; Li *et al.* 2025). Second, as discussed in § 3.4, the present data are also compatible with the scaling $St \sim (d_p/\eta)^{2/3}$ predicted by the spatial filtering ansatz (also shown in figure 6*a*).

Keeping in mind such caveats, we evaluate St via (3.3) and test the temporal filtering predictions (1.7) to (1.9). Here, we take $\boldsymbol{u}_{fp} = \boldsymbol{u}$, i.e. we assume that the particles do not preferentially sample flow regions with specific properties. This is supported by the evidence that finite-size neutrally buoyant particles do not cluster (Fiabane *et al.* 2012) or do so weakly (Uhlmann & Chouippe 2017). In figures 7(*a*) and 7(*b*), we then compare the measured fluctuating energy and correlation time scales of the floating particles against the temporal filtering predictions. Overall, the trend of $\langle u_p^2\rangle$ is correctly captured. The energy of the small particles is somewhat underestimated, likely because (3.3) overestimates their response time as mentioned previously. Larger discrepancies in $\langle u_p^2\rangle$ are found for $Re_\lambda = 29$, which might be due to the lack of scale separation of the inertial subrange in this case. The correlation time T_p is somewhat underestimated, although the experimental scatter for the larger particles (due to the limited number of long trajectories recorded) may partly account for the mismatch. Multiplying (1.7) and (1.9) yields

$$\frac{K_p}{K_t} = \frac{\langle u_p^2\rangle T_p}{\langle u^2\rangle T_L} = \frac{T_1 + T_2}{T_L} \sim 1, \tag{3.4}$$

i.e. the diffusivity is expected to be independent of the particle inertia (as originally predicted by Tchen 1947). That is, under the temporal filtering assumption, the increase of T_p/T_L with particle size balances the decrease of $\langle u_p^2\rangle/\langle u^2\rangle$. This prediction is consistent with the measurements at $Re_\lambda = 29$, while it underestimates the diffusivity measured in stronger turbulence, as shown in figure 7(*c*). There, the diffusivity is evaluated indirectly based on (3.4), i.e. as the product between the velocity variance and the correlation time scale rather than differentiating the mean square displacement, due to the limited length of the trajectories. Still, considering the vast range of particle sizes, the change in diffusivity is relatively modest, implying that (3.4) is a reasonable first-order approximation.

Figure 8(*a*) compares the measured particle acceleration variance and the trend predicted by (1.8). The general trend is captured, though with some quantitative discrepancies. We note that, in the inertial subrange, the temporal filtering framework

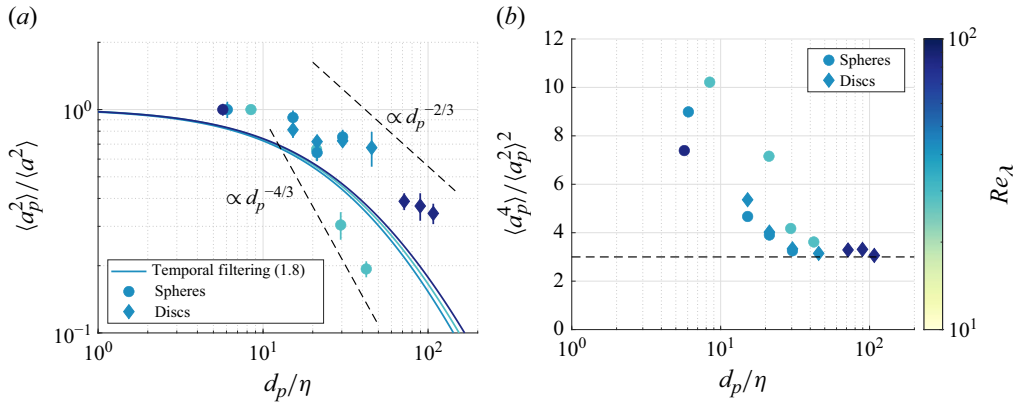

Figure 8. (*a*) Comparison between the measured particle acceleration variance (filled symbols) and the temporal filtering framework (1.8) (lines) for all Re_λ cases. Error bars represent the run-to-run standard deviation and the different power-law scalings are indicated by dashed lines. (*b*) Particle acceleration flatness as a function of dimensionless particle size. The dashed line indicates a flatness of 3, the value for a Gaussian distribution.

implies $\langle a_p^2\rangle/\langle a^2\rangle \sim St^{-1}$ (Berk & Coletti 2024), which according to the assumed linear relation (3.3) is equivalent to $\langle a_p^2\rangle/\langle a^2\rangle \sim (d_p/\eta)^{-1}$. Recent particle-resolved simulations in 3-D turbulence by Jiang *et al.* (2022) agree with such scaling. The present data, however, suggest an influence of Re_λ on the scaling, which will be discussed in § 3.4.

Finally, we consider the return to Gaussianity of the acceleration p.d.f.s for increasingly inertial particles, which is a hallmark of temporal filtering of small inertial particles in turbulence (Bec *et al.* 2006). This is quantified by the flatness $\langle a_p^4\rangle/\langle a_p^2\rangle^2$ plotted in figure 8(*b*), showing that intermittency in the floating particle acceleration is significant up to approximately $d_p/\eta = 50$. According to (3.3), this corresponds to $St \sim 5$. The temporal filtering framework does not provide *a priori* scaling for $\langle a_p^4\rangle/\langle a_p^2\rangle^2$, but we can refer to point-particle simulations based on such an assumption. For example, in the homogeneous 3-D turbulence simulations by Ireland *et al.* (2016) at $Re_\lambda = 88$ (comparable to our more turbulent case), the acceleration flatness approximately recovers the Gaussian value of 3 for $St \sim 10$ (see their figure 11).

3.4. *Comparison with the spatial filtering framework*

As discussed in § 1.2, the prevalent view is that neutrally buoyant finite-size particles act as spatial filters of the local turbulent flow. We test such an assumption by considering the amount of energy contained in the flow at scales up to d_p. This is readily represented by the second-order Eulerian velocity structure function, $S_2^E(r) = \langle \|\boldsymbol{u}(\boldsymbol{r}_0 + \boldsymbol{r}) - \boldsymbol{u}(\boldsymbol{r}_0)\|^2\rangle$, which quantifies the turbulent kinetic energy contained in scales r and smaller (Davidson 2015). As the particle responds to the remaining turbulent energy $\langle q^2\rangle - (1/2)S_2^E(d_p)$, the kinematic relation $S_2^E(r) = 2\langle q^2\rangle[1 - R_u^E(r)]$ implies that the fluctuating kinetic energy of a finite-size particle is

$$\langle u_p^2\rangle(d_p) \sim \langle q^2\rangle R_u^E(d_p). \tag{3.5}$$

Following Kolmogorov (1941) theory, this argument similarly leads to $(\langle q^2\rangle - \langle u_p^2\rangle)/\langle q^2\rangle \sim (d_p/\eta)^{2/3}$ in the inertial subrange (Homann & Bec 2010; Uhlmann & Chouippe 2017). Alternatively, $\langle u_p^2\rangle$ can be estimated directly from (3.5) if a model for $R_u^E(r)$ is available based on the turbulence properties. Inspired again by Sawford (1991),

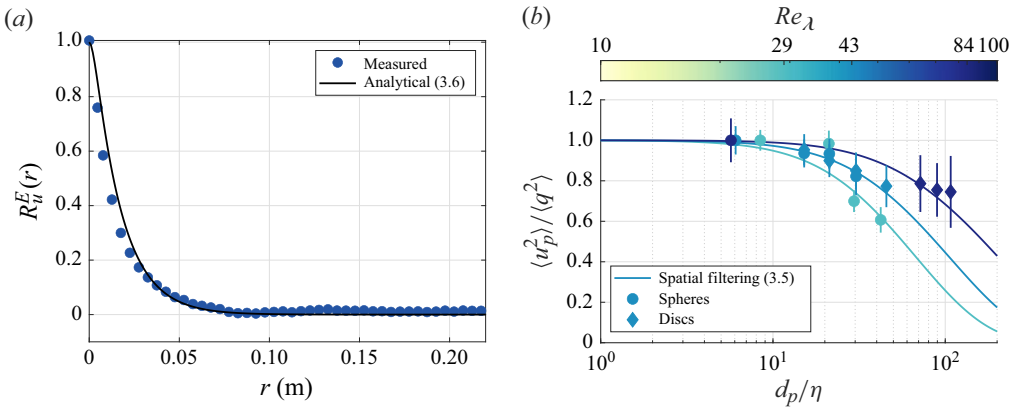

Figure 9. (*a*) Eulerian velocity autocorrelation coefficient for $Re_\lambda = 29$ measured by PTV (symbols) and in its analytical form (3.6). (*b*) Comparison between the measured particle fluctuating energy (filled symbols) and the spatial filtering framework (3.5) with (3.6).

we write a two-length exponential:

$$R_u^E(r) = \frac{L_1 e^{-r/L_1} - L_2 e^{-r/L_2}}{L_1 - L_2}, \tag{3.6}$$

where L_1 and L_2 are associated with the energy-containing and dissipative scales of the flow, respectively. Because $R_u^E(r)$ is expected to approximate a simple exponential in the large-scale limit, we take $L_1 = L$. Remembering that the Taylor microscale is related to the curvature of $R_u^E(r)$ at small scales (Pope 2000), we take $L_2 = \lambda$. This representation proves effective, reproducing well the measured Eulerian velocity autocorrelation coefficient, see figure 9(*a*). Remarkably, figure 9(*b*) shows that (3.5) captures the behaviour over the entire range of d_p/η and for all Re_λ considered here.

Let us now consider the other important properties of the particle motion, and their predicted trends based on the spatial filtering ansatz. While the application of Kolmogorov's theory leads to $\langle a_p^2\rangle/\langle a^2\rangle \sim (d_p/\eta)^{-2/3}$ (Voth *et al.* 2002), the question is complicated by the consideration that the forces acting on finite-size particles are driven by the pressure increments at their scale (Xu *et al.* 2007; Brown *et al.* 2009). The scaling for the latter is thought to vary with Re_λ, leading to a transition from $(d_p/\eta)^{-4/3}$ to $(d_p/\eta)^{-2/3}$ as the turbulence Reynolds number is increased (Qureshi *et al.* 2007; Homann & Bec 2010). The floating particle acceleration we measure at the different Re_λ (see figure 8*a*) agrees with this picture: the data at $Re_\lambda = 29$ are consistent with the $-4/3$ decay, whereas the more turbulent cases are compatible with the $-2/3$ decay.

Kolmogorov's inertial subrange theory also predicts the particle response time (taken as the correlation time scale of a_p) to scale as $\tau_p \sim \tau_\eta (d_p/\eta)^{2/3}$. Experiments and particle-resolved simulations of neutrally buoyant finite-size particles in 3-D turbulence, however, find only approximate agreement with such a trend, the comparison being complicated by the limited range of sizes and finite-Re_λ effects (Homann & Bec 2010; Volk *et al.* 2011; Uhlmann & Chouippe 2017; Jiang *et al.* 2022; Fan *et al.* 2024). Similarly, as shown in figure 6(*a*), our observations of floating particles are compatible with such inertial scaling, but do not allow us to unambiguously support it with respect to other proposals (such as (3.3)). Like previous studies, we are also limited to a marginal separation of scales, which in this case is inherent to the flow configuration: increasing the intensity of the free-surface turbulence inevitably leads to larger surface deformations, changing the nature of

the problem at hand (Brocchini & Peregrine 2001). Thus, unless fluids of high surface tension are used, turbulent motion along a quasi-flat free-surface can only be obtained at relatively small Re_λ.

The acceleration flatness can also be estimated in the framework of spatial filtering by assuming intermittency corrections for the high-order moments of the velocity increments (Volk *et al.* 2011; Fan *et al.* 2024). For example, using the model by She & Leveque (1994) leads to $\langle a_p^4\rangle/\langle a^2\rangle^2 \sim (d_p/\eta)^{-0.56}$. While this is comparable with the trends reported by Volk *et al.* (2011), the acceleration intermittency of finite-size neutrally buoyant particles in 3-D turbulence remains strong for all sizes: the flatness of the acceleration p.d.f. has consistently been reported to be much larger than 3, and often larger than 10, even for $d_p/\eta > 40$ (Qureshi *et al.* 2007, 2008; Xu & Bodenschatz 2008; Brown *et al.* 2009; Homann & Bec 2010; Volk *et al.* 2011; Bellani & Variano 2012; Uhlmann & Chouippe 2017; Jiang *et al.* 2022; Fan *et al.* 2024). Such a persistent intermittency for particle sizes so deep in the inertial subrange is contrary to a simplistic application of either the temporal or spatial filtering assumption (Qureshi *et al.* 2007). Strikingly, unlike in 3-D turbulence, particles floating on the free-surface do display a return to Gaussian acceleration p.d.f. with increasing size (see figures 4*a* and 8*b*).

The spatial filtering assumption does not offer a specific prediction for the Lagrangian dispersion, in particular, for T_p and K_p, nor are we aware of systematic studies of $R^L_{u_p}(\tau)$ and its decay for large particles in 3-D turbulence. The exception is represented by the study of Machicoane & Volk (2016), who measured $R^L_{u_p}(\tau)$ in a von Kármán flow. They found, however, that the confined nature of the flow crucially influenced $R^L_{u_p}(\tau)$, not allowing one to isolate the effect of particle size.

4. Discussion and conclusions

We have studied experimentally the behaviour of finite-size, marginally buoyant spheres and discs in homogeneous isotropic free-surface turbulence. By using two experimental facilities of identical architecture but different in size, we have spanned a wide range of parameters, with particle sizes up to $d_p/\eta \sim 100$ and turbulence Reynolds numbers $Re_\lambda \in [29, 84]$. The latter is limited by our focus on a regime of quasi-flat free-surfaces, without adding to this already complex system the effect(s) of wind shear and/or surface waves (Falkovich *et al.* 2005; Farazmand & Sapsis 2019; Del Grosso *et al.* 2019). The motion of the particles is compared with the behaviour of small floating tracers in the same free-surface flows. We find that the behaviour of particle diameters up to approximately $d_p/L = 0.1$ and/or $d_p/\eta = \mathcal{O}(10)$ is virtually indistinguishable from that of the free-surface flow. For larger sizes, the particle fluctuating energy $\langle u_p^2\rangle$ and acceleration variance $\langle a_p^2\rangle$ decrease, while their velocity correlation time T_p and response time τ_p (taken as the correlation time scale of the particle acceleration) increase. The opposite and comparable changes in $\langle u_p^2\rangle$ and T_p imply that the long-term diffusivity $K_p = \langle u_p^2\rangle T_p$ is weakly dependent on particle size. The accelerations become less intermittent with increasing particle size, displaying a Gaussian distribution above approximately $d_p/\eta = 50$. The present data show no systematic differences between spheres and discs when the diameter d_p (i.e. their maximum extension in the surface-parallel direction) is used to characterise their size. This indicates that the motion is mostly influenced by the near-surface flow, unlike non-spherical particles in 3-D turbulence for which the relevant geometric scale is the volume-equivalent diameter (Jiang *et al.* 2022).

We have used our measurements to address the question of whether, and to which degree, the motion of finite-size floating particles can be described by the two

fundamentally different approaches commonly used to rationalise the behaviour of inertial particles in turbulence: temporal filtering, which assumes that the particles respond only to fluid fluctuations slower than τ_p; and spatial filtering, which assumes that the particles respond only to fluctuations of length scale larger than d_p. In particular, we have applied the temporal filtering approach in its simplified form that assumes the particles to sample the flow ergodically, i.e. without favouring specific flow regions. This was the original assumption of Tchen (1947), which fails to capture important trends of small heavy particles that preferentially sample the turbulence (Wang & Stock 1993; Jung *et al.* 2008). In the case of large particles, however, the evidence from 3-D turbulence studies suggests that preferential sampling is weak. Under this assumption, the temporal filtering model provides closed expressions for the particle fluctuating energy, acceleration, velocity correlation time scale and diffusivity, based solely on τ_p and the characteristic time scales of the free-surface flow.

Our observations suggest that, in the present range of parameters, the response time (hence, the Stokes number) of the floating particles is reasonably estimated from d_p via an empirical linear relation derived for finite-size particles in 3-D turbulence. Using that, the temporal filtering approach captures the main observed trends of the transport properties. This is noteworthy, in that a simple particle equation of motion such as (1.5) is very useful in predicting the fate of floating particles in a free-surface flow of known properties. The diffusivity is especially important to parametrise the sub-grid terms in coarse-graining strategies (e.g. in large-eddy simulations and in other large-scale models used to predict the fate of marine pollution) but is usually poorly constrained. For example, in the study of Lagrangian transport of floating plastics in the Mediterranean Sea by Kaandorp *et al.* (2020), a range of K_p between 1 $\mathrm{m^2 s^{-1}}$ and 100 $\mathrm{m^2 s^{-1}}$ was considered. The prediction that particle diffusivity is, to first order, equal to that of the underlying free-surface turbulence (at least in the considered case of no wind and negligible waves) may prove useful in this sense.

The spatial filtering approach, however, is found to reproduce with quantitative accuracy the reduction of the fluctuating energy of the floating particles with increasing size. In particular, we stress the usefulness of the simple relation $\langle u_p^2 \rangle \sim \langle q^2 \rangle R_u^E(d_p)$ when the spatial autocorrelation of the free-surface flow is available or can be modelled. Here, we find it to be well represented by a two-length exponential inspired by Sawford's two-time model for the temporal autocorrelation. This framework predicts power-law scaling relations for the acceleration variance that are compatible with our observations, including the effect of Re_λ.

It is remarkable that the acceleration distributions of the floating particles lose their intermittent character with increasing size. This is consistent with the picture of both temporal and spatial filtering, but in contrast with observations in 3-D turbulence: there, the intermittency remains strong for neutrally buoyant particles of all sizes, indicating that any filtering approach (temporal or spatial) is inadequate or anyway too simplistic (Qureshi *et al.* 2007). The present finding suggests that finite-size floating particles may be more amenable to such representations.

The different acceleration distributions of large particles in free-surface versus 3-D flows may be interpreted in view of differences in the turbulent dynamics. In 3-D flows, the intense small-scale activity is correlated with large-scale fluctuations of the energy input (Blum *et al.* 2010, 2011; Carter & Coletti 2018; Vela-Martín & Avila 2024) and small vortices are often spatially organised around large-scale shear layers between energetic eddies (Ishihara, Gotoh & Kaneda 2009; Hunt *et al.* 2014). This may partly explain why even particles with inertial subrange sizes exhibit intermittent accelerations. In free-surface turbulence, while large-scale properties such as the turbulent kinetic energy and

the integral scales reflect those of the bulk (Li *et al.* 2025), the velocity gradient tensor of the surface motion follows profoundly different dynamics associated with the specific boundary conditions (Qi *et al.* 2025*b*). In particular, the free-surface vorticity and strain rate evolve over time scales comparable to T_L (rather than τ_η as in 3-D turbulence) and are related to upwelling/downwelling events moving fluid towards and away from the surface (Kumar *et al.* 1998; Shen *et al.* 1999; Lovecchio *et al.* 2015; Ruth & Coletti 2024; Li *et al.* 2025; Qi *et al.* 2025*a*). The equilibrium between upwellings and downwellings implies that stretching and compression of the surface-attached vortices are in balance (unlike in 3-D turbulence; Davidson 2015), impacting the organisation of the intense-fluctuation events and the inter-scale energy transfer along the free-surface (Ruth & Coletti 2024; Qi *et al.* 2025*a*,*b*). Further studies that simultaneously capture both the flow and the particle motion shall elucidate how the spatio-temporal structure of the turbulence affects the acceleration of finite-size floating particles.

Taken together, these results demonstrate that both the temporal filtering and the spatial filtering approaches capture important and complementary aspects of the motion of floating particles in free-surface turbulence. Spatial filtering provides a more accurate estimate of the decrease in particle fluctuating energy with size, compared with the prediction based on temporal filtering. The relative success of the latter might actually be rooted in the approximately linear relation between d_p and τ_p, and thus merely reflect spatial filtering. Temporal filtering, however, also yields approximate estimates of the velocity correlation time scale and diffusivity, which are not directly predicted by spatial filtering. As Tchen (1947) first realised, the concept of response time and temporal filtering are intertwined and, as such, temporal filtering is implicit in point-particle simulations of Lagrangian transport based on (1.5). The present findings suggest that, for finite-size floating particles, alternative approaches fully based on spatial filtering may be desirable, though defining them is outside the scope of the present work. Finally, we remark on an important limitation: for the considered case of negligible waves to be realised, Re_λ (and thus scale separation) cannot be large. This implies that scaling relations such as those predicted by spatial filtering using Kolmogorov's theory have a limited range of applicability. Such a limitation on the Reynolds number, in turn, constrains the scale separation in the flow. Therefore, one cannot clearly discern whether the relevant dimensionless particle size is d_p/L, d_p/η or possibly d_p/λ. From basic notions on turbulent kinetic energy and intermittency, the behaviour of the particle velocity and acceleration are expected to depend on the size compared with the integral and Kolmogorov scale, respectively. This may be a simplistic view, considering the relations between distance scales (Blum *et al.* 2011) and the peculiar nature of the free-surface (Qi *et al.* 2025*a*).

Future works shall explore further the influence of floating particle geometry, for example, considering prolate particles whose translation and rotational motions are coupled (Voth & Soldati 2017) and which represent a large fraction of marine plastics (Kooi & Koelmans 2019). Moreover, research is warranted on how the effect of turbulence combines with that of surface waves, whose impact on the transport of spherical and non-spherical particles has attracted significant interest in recent years (Pizzo, Melville & Deike 2019; Baker & DiBenedetto 2023; Xiao *et al.* 2024). Finally, in the presence of wind, the submergence will determine the influence of windage, i.e. the drag experienced by objects partly protruding above the free-surface (Beron-Vera, Olascoaga & Miron 2019).

Acknowledgements. The authors gratefully acknowledge the support of R. Vonbank for their assistance with the water channel at Empa.

Funding. The present work was supported by the Swiss National Science Foundation (Project No. 207318)

Declaration of interests. The authors report no conflict of interest.

Data availability statement. The corresponding author makes all the data supporting this work available upon reasonable request.

References

Aarnes, J.R., Babiker, O.M., Xuan, A., Shen, L., Ellingsen, S.Å. 2025 Vortex structures under dimples and scars in turbulent free-surface flows. *J. Fluid Mech.* **1007**, A38.

Baker, L. & DiBenedetto, M. 2023 Large-scale particle shadow tracking and orientation measurement with collimated light. *Exp. Fluids* **64** (3), 52.

Baker, L.J. & Coletti, F. 2019 Experimental study of negatively buoyant finite-size particles in a turbulent boundary layer up to dense regimes. *J. Fluid Mech.* **866**, 598–629.

Baker, L.J. & Coletti, F. 2021 Particle–fluid–wall interaction of inertial spherical particles in a turbulent boundary layer. *J. Fluid Mech.* **908**, A39.

Baker, L.J. & Coletti, F. 2022 Experimental investigation of inertial fibres and disks in a turbulent boundary layer. *J. Fluid Mech.* **943**, A27.

Balachandar, S. 2009 A scaling analysis for point–particle approaches to turbulent multiphase flows. *Intl J. Multiphase Flow* **35** (9), 801–810.

Balachandar, S. & Eaton, J.K. 2010 Turbulent dispersed multiphase flow. *Annu. Rev. Fluid Mech.* **42**, 111–133.

Batchelor, G.K. 1957 Diffusion in free turbulent shear flows. *J. Fluid Mech.* **3** (1), 67–80.

Bec, J., Biferale, L., Boffetta, G., Celani, A., Cencini, M., Lanotte, A., Musacchio, S. & Toschi, F. 2006 Acceleration statistics of heavy particles in turbulence. *J. Fluid Mech.* **550**, 349–358.

Bellani, G. & Variano, E.A. 2012 Slip velocity of large neutrally buoyant particles in turbulent flows. *New J. Phys.* **14** (12), 125009.

Berk, T. & Coletti, F. 2021 Dynamics of small heavy particles in homogeneous turbulence: a Lagrangian experimental study. *J. Fluid Mech.* **917**, A47.

Berk, T. & Coletti, F. 2024 An analytical model for the slip velocity of particles in turbulence. *J. Fluid Mech.* **996**, A1.

Beron-Vera, F.J. 2024 Dynamics of inertial particles on the ocean surface with unrestricted reserve buoyancy. *Phys. Fluids* **36** (10), 101702.

Beron-Vera, F.J., Olascoaga, M.J. & Miron, P. 2019 Building a Maxey–Riley framework for surface ocean inertial particle dynamics. *Phys. Fluids* **31** (9), 096602.

Blum, D.B., Bewley, G.P., Bodenschatz, E., Gibert, M., Gylfason, Á., Mydlarski, L., Voth, G.A., Xu, H. & Yeung, P.K. 2011 Signatures of non-universal large scales in conditional structure functions from various turbulent flows. *New J. Phys.* **13** (11), 113020.

Blum, D.B., Kunwar, S.B., Johnson, J. & Voth, G.A. 2010 Effects of nonuniversal large scales on conditional structure functions in turbulence. *Phys. Fluids* **22** (1), 015107.

Boffetta, G., Davoudi, J., Eckhardt, B. & Schumacher, J. 2004 Lagrangian tracers on a surface flow: the role of time correlations. *Phys. Rev. Lett.* **93**, 134501.

Bonner, G., Beron-Vera, F.J. & Olascoaga, M.J. 2024 Charting the course of *Sargassum* : incorporating nonlinear elastic interactions and life cycles in the Maxey–Riley model. *PNAS Nexus* **3** (10), pgae451.

Brandt, L. & Coletti, F. 2022 Particle-laden turbulence: progress and perspectives. *Annu. Rev. Fluid Mech.* **54**, 159–189.

Brocchini, M. & Peregrine, D.H. 2001 The dynamics of strong turbulence at free surfaces. Part 1. Description. *J. Fluid Mech.* **449**, 225–254.

Brown, R.D., Warhaft, Z. & Voth, G.A. 2009 Acceleration statistics of neutrally buoyant spherical particles in intense turbulence. *Phys. Rev. Lett.* **103** (19), 194501.

Calzavarini, E., Volk, R., Bourgoin, M., Lévêque, E., Pinton, J.-F. & Toschi, F. 2009 Acceleration statistics of finite-sized particles in turbulent flow: the role of Faxén forces. *J. Fluid Mech.* **630**, 179–189.

Calzavarini, E., Volk, R., Lévêque, E., Pinton, J.-F. & Toschi, F. 2012 Impact of trailing wake drag on the statistical properties and dynamics of finite-sized particle in turbulence. *Phys. D: Nonlinear Phenom.* **241** (3), 237–244.

Carter, D.W. & Coletti, F. 2018 Small-scale structure and energy transfer in homogeneous turbulence. *J. Fluid Mech.* **854**, 505–543.

Chouippe, A. & Uhlmann, M. 2015 Forcing homogeneous turbulence in direct numerical simulation of particulate flow with interface resolution and gravity. *Phys. Fluids* **27** (12), 123301.

CLIFT, R., GRACE, J.R. & WEBER, M.E. 2005 Bubbles, drops, and particles.
CRESSMAN, J.R., DAVOUDI, J., GOLDBURG, W.I. & SCHUMACHER, J. 2004 Eulerian and Lagrangian studies in surface flow turbulence. *New J. Phys.* **6** (1), 53.
CSANADY, G.T. 1963 Turbulent diffusion of heavy particles in the atmosphere. *J. Atmos. Sci.* **20** (3), 201–208.
DAVIDSON, P. 2015 *Turbulence: an Introduction for Scientists and Engineers*. Oxford University Press.
DEL GROSSO, N.F., CAPPELLETTI, L.M., SUJOVOLSKY, N.E., MININNI, P.D. & COBELLI, P.J. 2019 Statistics of single and multiple floaters in experiments of surface wave turbulence. *Phys. Rev. Fluids* **4** (7), 074805.
FALKOVICH, G., WEINBERG, A., DENISSENKO, P. & LUKASCHUK, S. 2005 Floater clustering in a standing wave. *Nature* **435** (7045), 1045–1046.
FAN, Y., WANG, C., JIANG, L., SUN, C. & CALZAVARINI, E. 2024 Accelerations of large inertial particles in turbulence. *Europhys. Lett.* **145** (4), 43001.
FARAZMAND, M. & SAPSIS, T. 2019 Surface waves enhance particle dispersion. *Fluids* **4** (1), 55.
FIABANE, L., ZIMMERMANN, R., VOLK, R., PINTON, J.-F. & BOURGOIN, M. 2012 Clustering of finite-size particles in turbulence. *Phys. Rev. E* **86** (3), 035301.
GEYER, R., JAMBECK, J.R. & LAW, K.L. 2017 Production, use, and fate of all plastics ever made. *Sci. Adv.* **3** (7), e1700782.
GRIFFA, A. 1996 Applications of stochastic particle models to oceanographic problems. In *Stochastic Modelling in Physical Oceanography*, pp. 113–140. Springer.
GUALA, M., LIBERZON, A., TSINOBER, A. & KINZELBACH, W. 2007 An experimental investigation on Lagrangian correlations of small-scale turbulence at low Reynolds number. *J. Fluid Mech.* **574**, 405–427.
GUO, X. & SHEN, L. 2010 Interaction of a deformable free surface with statistically steady homogeneous turbulence. *J. Fluid Mech.* **658**, 33–62.
HEARST, R.J. & LAVOIE, P. 2014 Decay of turbulence generated by a square-fractal-element grid. *J. Fluid Mech.* **741**, 567–584.
HINZE, J.O. 1975 *Turbulence*. McGraw-Hill.
HOMANN, H. & BEC, J. 2010 Finite-size effects in the dynamics of neutrally buoyant particles in turbulent flow. *J. Fluid Mech.* **651**, 81–91.
HUCK, P.D., MACHICOANE, N. & VOLK, R. 2019 Lagrangian acceleration timescales in anisotropic turbulence. *Phys. Rev. Fluids* **4** (6), 064606.
HUNT, J.C.R. & GRAHAM, J.M.R. 1978 Free-stream turbulence near plane boundaries. *J. Fluid Mech.* **84** (2), 209–235.
HUNT, J.C.R., ISHIHARA, T., WORTH, N.A. & KANEDA, Y. 2014 Thin shear layer structures in high Reynolds number turbulence: tomographic experiments and a local distortion model. *Flow Turbul. Combust.* **92** (3), 607–649.
IRELAND, P.J., BRAGG, A.D. & COLLINS, L.R. 2016 The effect of Reynolds number on inertial particle dynamics in isotropic turbulence. Part 1. Simulations without gravitational effects. *J. Fluid Mech.* **796**, 617–658.
ISHIHARA, T., GOTOH, T. & KANEDA, Y. 2009 Study of high–Reynolds number isotropic turbulence by direct numerical simulation. *Annu. Rev. Fluid Mech.* **41** (1), 165–180.
JIANG, L., WANG, C., LIU, S., SUN, C. & CALZAVARINI, E. 2022 Dynamics of finite-size spheroids in turbulent flow: the roles of flow structures and particle boundary layers. *J. Fluid Mech.* **939**, A22.
JIMÉNEZ, J. 1997 Oceanic turbulence at millimeter scales. *Sci. Mar.* **61**, 47–56.
JUNG, J., YEO, K. & LEE, C. 2008 Behavior of heavy particles in isotropic turbulence. *Phys. Rev. E Stat. Nonlinear Soft Matt. Phys.* **77** (1), 016307.
KAANDORP, M.L.A., DIJKSTRA, H.A. & VAN SEBILLE, E. 2020 Closing the mediterranean marine floating plastic mass budget: inverse modeling of sources and sinks. *Environ. Sci. Technol.* **54** (19), 11980–11989.
KAANDORP, M.L.A., LOBELLE, D., KEHL, C., DIJKSTRA, H.A. & VAN SEBILLE, E. 2023 Global mass of buoyant marine plastics dominated by large long-lived debris. *Nat. Geosci.* **16** (8), 689–694.
KIDANEMARIAM, A.G., CHAN-BRAUN, C., DOYCHEV, T. & UHLMANN, M. 2013 Direct numerical simulation of horizontal open channel flow with finite-size, heavy particles at low solid volume fraction. *New J. Phys.* **15** (2), 025031.
KOLMOGOROV, A.N. 1941 The local structure of turbulence in incompressible viscous fluid for very large Reynolds numbers. In Proceedings of the URSS Academy of Sciences, vol. **30**, pp. 301–305
KOOI, M. & KOELMANS, A.A. 2019 Simplifying microplastic via continuous probability distributions for size, shape, and density. *Environ. Sci. Tech. Lett.* **6** (9), 551–557.
KUMAR, S., GUPTA, R. & BANERJEE, S. 1998 An experimental investigation of the characteristics of free-surface turbulence in channel flow. *Phys. Fluids* **10** (2), 437–456.
LAVOIE, P., DJENIDI, L. & ANTONIA, R.A. 2007 Effects of initial conditions in decaying turbulence generated by passive grids. *J. Fluid Mech.* **585**, 395–420.

LI, Y., SALMON SANNESS, H., HASSAINI, R., CHANG, K., MUCIGNAT, C. & COLETTI, F. 2025 Spatiotemporal scales of motion and particle clustering in free-surface turbulence. *Phys. Rev. Fluids* **10**, 034602.

LI, Y., WANG, Y., QI, Y. & COLETTI, F. 2024 Relative dispersion in free-surface turbulence. *J. Fluid Mech.* **993**, R2.

LING, Y., PARMAR, M. & BALACHANDAR, S. 2013 A scaling analysis of added-mass and history forces and their coupling in dispersed multiphase flows. *Intl J. Multiphase Flow* **57**, 102–114.

LOVECCHIO, S., MARCHIOLI, C. & SOLDATI, A. 2013 Time persistence of floating-particle clusters in free-surface turbulence. *Phys. Rev. E* **88**, 033003.

LOVECCHIO, S., ZONTA, F. & SOLDATI, A. 2015 Upscale energy transfer and flow topology in free-surface turbulence. *Phys. Rev. E* **91**, 033010.

MACHICOANE, N., HUCK, P.D. & VOLK, R. 2017 Estimating two-point statistics from derivatives of a signal containing noise: application to auto-correlation functions of turbulent Lagrangian tracks. *Rev. Sci. Instrum.* **88** (6), 065113.

MACHICOANE, N. & VOLK, R. 2016 Lagrangian velocity and acceleration correlations of large inertial particles in a closed turbulent flow. *Phys. Fluids* **28** (3), 035113.

MACHICOANE, N., ZIMMERMANN, R., FIABANE, L., BOURGOIN, M., PINTON, J.-F. & VOLK, R. 2014 Large sphere motion in a nonhomogeneous turbulent flow. *New J. Phys.* **16** (1), 013053.

MAGNAUDET, J. 2003 High-Reynolds-number turbulence in a shear-free boundary layer: revisiting the Hunt–Graham theory. *J. Fluid Mech.* **484**, 167–196.

MATHAI, V., LOHSE, D. & SUN, C. 2020 Bubbly and buoyant particle–laden turbulent flows. *Annu. Rev. Condens. Matt. Phys.* **11** (1), 529–559.

MAXEY, M.R. 1987 The gravitational settling of aerosol particles in homogeneous turbulence and random flow fields. *J. Fluid Mech.* **174**, 441–465.

MEHRABADI, M., HORWITZ, J.A.K., SUBRAMANIAM, S. & MANI, A. 2018 A direct comparison of particle-resolved and point-particle methods in decaying turbulence. *J. Fluid Mech.* **850**, 336–369.

MOHAMED, M.S. & LARUE, J.C. 1990 The decay power law in grid-generated turbulence. *J. Fluid Mech.* **219**, 195–214.

MORDANT, N., CRAWFORD, A.M. & BODENSCHATZ, E. 2004*a* Experimental Lagrangian acceleration probability density function measurement. *Physica D: Nonlinear Phenom.* **193** (1-4), 245–251.

MORDANT, N., LÉVÊQUE, E. & PINTON, J.-F. 2004*b* Experimental and numerical study of the Lagrangian dynamics of high Reynolds turbulence. *New J. Phys.* **6** (1), 116.

NIKORA, V., NOKES, R., VEALE, W., DAVIDSON, M. & JIRKA, G.H. 2007 Large-scale turbulent structure of uniform shallow free-surface flows. *Environ. Fluid Mech.* **7** (2), 159–172.

OUELLETTE, N.T., O'MALLEY, P.J.J. & GOLLUB, J.P. 2008 Transport of finite-sized particles in chaotic flow. *Phys. Rev. Lett.* **101** (17), 174504.

PEROT, B. & MOIN, P. 1995 Shear-free turbulent boundary layers. Part 1. Physical insights into near-wall turbulence. *J. Fluid Mech.* **295**, 199–227.

PIZZO, N., MELVILLE, W.K. & DEIKE, L. 2019 Lagrangian transport by nonbreaking and breaking deep-water waves at the ocean surface. *J. Phys. Oceanogr.* **49** (4), 983–992.

POPE, S.B. 2000 *Turbulent Flows*. Cambridge University Press.

QI, Y., LI, Y. & COLETTI, F. 2025*a* Small-scale dynamics and structure of free-surface turbulence. *J. Fluid Mech.* **1007**, A3.

QI, Y., XU, Z. & COLETTI, F. 2025*b* Restricted euler dynamics in free-surface turbulence. *J. Fluid Mech.* **1002**, A38.

QURESHI, N.M., ARRIETA, U., BAUDET, C., CARTELLIER, A., GAGNE, Y. & BOURGOIN, M. 2008 Acceleration statistics of inertial particles in turbulent flow. *Eur. Phys. J. B* **66**, 531–536.

QURESHI, N.M., BOURGOIN, M., BAUDET, C., CARTELLIER, A. & GAGNE, Y. 2007 Turbulent transport of material particles: an experimental study of finite size effects. *Phys. Rev. Lett.* **99** (18), 184502.

RUTH, D.J. & COLETTI, F. 2024 Structure and energy transfer in homogeneous turbulence below a free surface. *J. Fluid Mech.* **1001**, A46.

SANNESS SALMON, H.R., BAKER, L.J., KOZAREK, J.L. & COLETTI, F. 2023 Effect of shape and size on the transport of floating particles on the free surface in a natural stream. *Water Resour. Res.* **59** (10), e2023WR035716.

SAWFORD, B.L. 1991 Reynolds number effects in Lagrangian stochastic models of turbulent dispersion. *Phys. Fluids A: Fluid Dyn.* **3** (6), 1577–1586.

SHE, Z.-S. & LEVEQUE, E. 1994 Universal scaling laws in fully developed turbulence. *Phys. Rev. Lett.* **72** (3), 336.

SHEN, L., ZHANG, X., YUE, D.K.P. & TRIANTAFYLLOU, G.S. 1999 The surface layer for free-surface turbulent flows. *J. Fluid Mech.* **386**, 167–212.
SINHUBER, M., BODENSCHATZ, E. & BEWLEY, G.P. 2015 Decay of turbulence at high Reynolds numbers. *Phys. Rev. Lett.* **114** (3), 034501.
SQUIRES, K.D. & EATON, J.K. 1991 Measurements of particle dispersion obtained from direct numerical simulations of isotropic turbulence. *J. Fluid Mech.* **226**, 1–35.
TAYLOR, G.I. 1922 Diffusion by continuous movements. *Proc. Lond. Math. Soc.* **2** (1), 196–212.
TCHEN, C.-M. 1947 *Mean Value and Correlation Problems Connected with the Motion of Small Particles Suspended in a Turbulent Fluid*. Springer Dordrecht.
TENNEKES, H. & LUMLEY, J.L. 1972 *A First Course in Turbulence*. MIT press.
TOSCHI, F. & BODENSCHATZ, E. 2009 Lagrangian properties of particles in turbulence. *Annu. Rev. Fluid Mech.* **41** (1), 375–404.
UHLMANN, M. & CHOUIPPE, A. 2017 Clustering and preferential concentration of finite-size particles in forced homogeneous-isotropic turbulence. *J. Fluid Mech.* **812**, 991–1023.
UHLMANN, M. & DOYCHEV, T. 2014 Sedimentation of a dilute suspension of rigid spheres at intermediate Galileo numbers: the effect of clustering upon the particle motion. *J. Fluid Mech.* **752**, 310–348.
VALERO, D., BELAY, B.S., MORENO-RODENAS, A., KRAMER, M. & FRANCA, M.J. 2022 The key role of surface tension in the transport and quantification of plastic pollution in rivers. *Water Res.* **226**, 119078.
VELA-MARTÍN, A. & AVILA, M. 2024 Large-scale patterns set the predictability limit of extreme events in Kolmogorov flow. *J. Fluid Mech.* **986**, A2.
VIGGIANO, B., BASSET, T., SOLOVITZ, S., BAROIS, T., GIBERT, M., MORDANT, N., CHEVILLARD, L., VOLK, R., BOURGOIN, M. & CAL, R.B. 2021 Lagrangian diffusion properties of a free shear turbulent jet. *J. Fluid Mech.* **918**, A25.
VOLK, R., CALZAVARINI, E., LEVEQUE, E. & PINTON, J.-F. 2011 Dynamics of inertial particles in a turbulent von Kármán flow. *J. Fluid Mech.* **668**, 223–235.
VOLK, R., CALZAVARINI, E., VERHILLE, G., LOHSE, D., MORDANT, N., PINTON, J.-F. & TOSCHI, F. 2008 Acceleration of heavy and light particles in turbulence: comparison between experiments and direct numerical simulations. *Phys. D: Nonlinear Phenom.* **237** (14-17), 2084–2089.
VOTH, G.A., LA, P., ARTHUR, C., ALICE, M., ALEXANDER, J. & BODENSCHATZ, E. 2002 Measurement of particle accelerations in fully developed turbulence. *J. Fluid Mech.* **469**, 121–160.
VOTH, G.A. & SOLDATI, A. 2017 Anisotropic particles in turbulence. *Annu. Rev. Fluid Mech.* **49** (1), 249–276.
WANG, L.-P. & STOCK, D. 1993 Dispersion of heavy particles by turbulent motion. *J. Atmos. Sci.* **50**, 1897–1913.
WILSON, J.D. & SAWFORD, B.L. 1996 Review of Lagrangian stochastic models for trajectories in the turbulent atmosphere. *Boundary-Layer Meteorol.* **78**, 191–210.
XIA, H., FRANCOIS, N., PUNZMANN, H. & SHATS, M. 2019 Tunable diffusion in wave-driven two-dimensional turbulence. *J. Fluid Mech.* **865**, 811–830.
XIAO, Q., CALVERT, R., YAN, S.Q., ADCOCK, T.A.A. & VAN DEN BREMER, T.S. 2024 Surface gravity wave-induced drift of floating objects in the diffraction regime. *J. Fluid Mech.* **980**, A27.
XU, H. & BODENSCHATZ, E. 2008 Motion of inertial particles with size larger than Kolmogorov scale in turbulent flows. *Phys. D: Nonlinear Phenom.* **237** (14-17), 2095–2100.
XU, H., OUELLETTE, N.T., VINCENZI, D. & BODENSCHATZ, E. 2007 Acceleration correlations and pressure structure functions in high-Reynolds number turbulence. *Phys. Rev. Lett.* **99** (20), 204501.
YEUNG, P.-K. & POPE, S.B. 1989 Lagrangian statistics from direct numerical simulations of isotropic turbulence. *J. Fluid Mech.* **207**, 531–586.
ZHANG, Z. 2000 A flexible new technique for camera calibration. *IEEE Trans. Pattern Anal. Mach. Intell.* **22** (11), 1330–1334.